COMSOL
CONFERENCE
2024 FLORENCE

Simulating the Coupled Mass and Heat Transport in Packaging Material during Induction Sealing

H. Makungu Askfelt[1], G. Betti Beneventi[2], M. Alexandersson[1]
1. Tetra Pak Packaging Solutions AB, Lund, Sweden.
2. Tetra Pak Packaging Solutions S.p.A, Modena, Italy

Abstract
COMSOL Multiphysics is used to integrate the coupled heat and mass transport, within a package material, with electromagnetic induction. The resulting model is used to analyze the response of package material during induction heating. The capability of the model is analyzed via a parametric sweep, and it is shown that the model is able to capture complex multiphysical couplings such as how gauge pressure and drying are affected by the density and initial moisture ratio of the package material.
Keywords: Paperboard, Mixture theory, Coupled Mass and Heat Transport, Induction heating, Induction sealing.

Introduction
Packaging Material (PM), used for liquid food packages, has a layered structure typically similar to the one depicted in Figure 1.

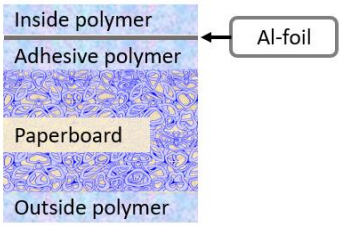

Figure 1. Conceptual illustration of the layered structure of a liquid food PM.

The processes of transforming PM into a filled package can look very different depending on the contained product and package design requirements. One step that is always included is the sealing(s) of the package. Different technologies for sealing exist and this paper focus on Induction Heating (IH) sealing where the PM is exposed to an alternating magnetic field, generating eddy currents in, and consequently heat, the Al-foil. During an IH-seal the temperature of the Al-foil typically elevates to > 150 °C in less than 1 s. The heat transfers to the inside polymer which melts and when two insides are pressed together and cooled a package seal is formed [1].

The rapid and significant heating of the PM is accompanied with several interesting physics such as; phase transformations (e.g. polymer melting, paperboard drying), mass transport (e.g. polymer movement and air seepage and vapor diffusion within the paperboard), heat transport (e.g. convective and conductive transport and energy release/storage related to enthalpy of phase change). Furthermore, these processes are coupled, and the IH-sealing process of a liquid food package classifies as a multi-physical problem. It can of course be argued that the IH-sealing process works fine today and that it is not necessary to describe all the physics or how they are coupled. However, the packaging industry is currently going through great changes in transitioning towards more sustainable PMs and more sustainable production processes. Moreover, these changes are occurring at a fast pace and virtual simulations is a vital tool assisting in the journey.

In this paper it is shown how *COMSOL Multiphysics* enables simulations of the non-trivial coupled physics occurring during an IH-sealing process of a liquid food package. Focus is on the IH-heating of the Al-foil and how this connects to the coupled mass and heat transport in the paperboard. The response of the paperboard is modeled using the Mixture Theory (MT) framework as outlined in [2]. The response of the polymer is simplified and neglects phase transformations as well as motions.

Experimental setup
In attempt to improve the understanding of the PM response during an IH-sealing operation, a sub-system test rig was designed in [3]. Compared to the sealing system in a filling machine, (FM), the test rig is simplified and focuses merely on how the PM is heated. The test rig consists of a relatively simple IH-system containing an aluminum inductor (here, made of a coil) and a generator. In contrast to a FM, the PM is fixed in position and held in place with biadhesive tape. The same tape is also used to set the relative position between the coil and the

PM. A 3D illustration of the coil is shown in Figure 2 and a 2D illustration of the central cross section of the coil, together with the biadhesive tape and the PM is shown in Figure 3.

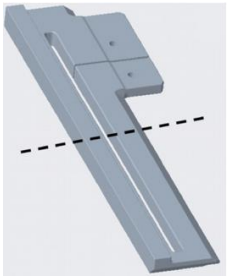

Figure 2. 3D illustration of the aluminum coil used in the sub-system test developed in [3]. Dashed-line: location of central cross-section (see Figure 3).

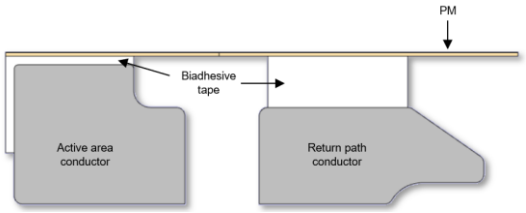

Figure 3. Illustration of the cross section of the sub-system test, including: coil, biadhesive tape, and PM.

The generator gives rise to a primary current in the coil, a single-tone sine wave of frequency $f \approx 500$ kHz and magnitude ≈ 100 A. According to Ampère's law, the alternating current (ac), generates a "primary" time-varying magnetic field, around the PM. From Faraday's equation, the magnetic field yields to electrical currents flowing in nearby conductive material, referred to as the "workpiece", here, the Al-foil of the PM. The currents form vortex-like paths, "eddy currents", which acts as heat sources in the Al-foil, commonly known as Joule heating. The eddy current in the Al-foil is an ac current with the same frequency f as the primary current and consequently an additional "secondary" time-varying magnetic field is generated. The net magnetic field, in space, is given by the superposition of primary and secondary fields.
As the Al-foil is heated, its electrical resistivity increases, and, for a fixed primary current, the power loss on the Al-foil would also increases with time. This means that the total load power delivered by the generator would increase as well during the heating transient. However, the sub system in [3] is set up with a closed-loop feedback system that reduces the primary current dynamically such that the total power on the IH load is constant during the whole heating transient

Theory

Al-foil: induction heating, and heat transport

The theoretic framework and numerical formulations of the electromagnetics of eddy currents are well-established, and a comprehensive review on the subject is given in [4].

The general format of the eddy current problem is described by the coupled Ampère and Faraday's laws which, in the frequency domain, read

$$\nabla \times \boldsymbol{H} = \boldsymbol{J} + j2\pi f \boldsymbol{D},$$
$$\nabla \times \boldsymbol{E} = -j2\pi f \boldsymbol{B}.$$

Here $\boldsymbol{H}$ [A/m] is the magnetic field, $\boldsymbol{J}=\sigma\boldsymbol{E}$ [A/m^2] the current density, $\boldsymbol{E}$ [V/m] the electric field, σ [S/m] the material electrical conductivity; $\boldsymbol{B}$ [T] the magnetic flux density, and $\boldsymbol{D}$ [C/m^2] the electric displacement. The primary variable of eddy currents problem is chosen as the magnetic vector potential $\boldsymbol{A}$ [Wb/m], which is defined by

$$\nabla \times \boldsymbol{A} = \boldsymbol{B}.$$

The cycle-average Joule heating source term Q_{IH} [W · m^{-3}], is retrieved through manipulation of Ampère's and Faraday's equations and reads

$$Q_{IH} = \frac{1}{2}\boldsymbol{E} \cdot \boldsymbol{J}^*,$$

where $\boldsymbol{J}^*$ is the complex conjugate of the induced current density.
Finally, the heat evolution in the Al-foil is governed by the following heat transport equation;

$$\rho_{AL} c_{AL}^p \dot{\theta} - \nabla \cdot \left(\lambda_{Al} \nabla(\theta)\right) - Q_{IH} = 0.$$

Here the notations $\dot{(\,)}$ [1/s] and ∇ [1/m] are used for the time derivative and gradient operator, respectively. Furthermore, θ [K] is the absolute temperature, λ_{Al}^p [W/m/K] is the thermal conductivity, ρ_{Al} [kg/m^3] the density, and c_{Al}^p [J/kg/K] the specific heat.

Polymer layers – heat transport

All three polymer-layers of the PM, see Figure 1, are assumed to behave as polyethylene (PE). Following the rapid nature of the IH-seal, the PE layers are considered impermeable, and the response of the PE-layers is governed by a heat equation of the same format as the Al-foil but without a heat source.

Paperboard - Coupled heat and mass transport
A complete presentation of the model assumed for the paperboard response is given in [2] and the following description is limited to important concepts and the governing equations. The model is founded in a MT framework and paperboard is viewed as a mixture of three immiscible phases; solid fibers $(\cdot)_s$, vicinal water $(\cdot)_l$, and pore space air $(\cdot)_g$. The gas phase is assumed to be a miscible mixture of dry air $(\cdot)_{g_a}$ and water vapor $(\cdot)_{g_v}$. A conceptual illustration is shown in Figure 4.

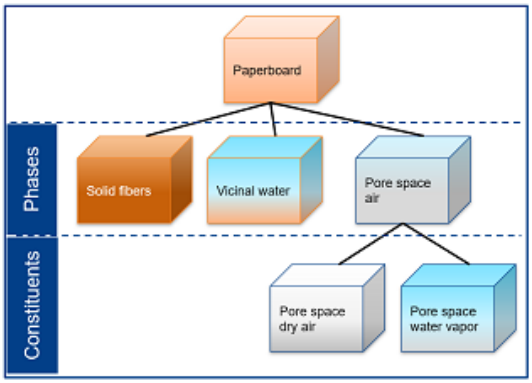

Figure 4. Conceptual illustration of the decomposition of the paperboard into immiscible phases and miscible constituents.

The response of the paperboard is governed by three balance of mass equations and one heat transport equation, given by;

Balance of mass vicinal water

$$\rho_s n_s \dot{\omega} + \hat{m}_{s:g} = 0$$

Balance of mass inter fiber dry air

$$\rho_{g_a}\dot{n}_g + \frac{n_g \rho_{g_a}}{p_{g_a}}\dot{p}_{g_a} - \frac{n_g \rho_{g_a}}{\theta}\dot{\theta} + \nabla \cdot \left(\mathbf{J}_{g_a}\right) = 0$$

Balance of mass inter fiber water vapor

$$\rho_{g_v}\dot{n}_g + \frac{n_g \rho_{g_v}}{p_{g_v}}\dot{p}_{g_v} - \frac{n_g \rho_{g_v}}{\theta}\dot{\theta} + \nabla \cdot \left(\mathbf{J}_{g_v}\right) - \hat{m}_{s:g} = 0$$

Heat transport – Mixture;

$$\rho_{PB} c_{PB}^{p}\dot{\theta} + \nabla \cdot \left(\boldsymbol{q}_{PB}^{\theta}\right) + \hat{m}_{s:g}\Delta H_{s:g} = 0$$

The following primary variables are selected: moisture ratio, ω [-], partial pressures of the dry air p_{g_a} [Pa] and water vapor p_{g_v} [Pa], and absolute temperature θ [K]. The reader is referred to [2], [5] for a complete description of constitutive relations, which are here presented with notation and unit;

n_α [-]: Volume fraction of α.
ρ_α, ρ_{g_j} [kg/m^3]: Densities of α and g_j.
$\hat{m}_{s:g}$ [kg/m^3/s]: Rate of phase change $s \rightarrow g$.
$\mathbf{J}_{g_j}$ [kg/m^2/s]: Total mass flux of g_j.
$\boldsymbol{q}_{PB}^{\theta}$ [W/m^2]: Total heat flux mixture.
$\Delta H_{s:g}$ [J/kg]: Enthalpy required of $\hat{m}_{s:g}$

Numerical Model

The virtual representation of a sub-system test execution is implemented with two steps; Step1) a 600 ms long *Frequency-Transient* study describing the heating of the PM and Step2) a 9 400 ms long *Time Dependent* step describing the cool down.

Geometry

The adopted computational domain is presented in Figure 5. Due to the differences in length scale, the figure contains two zoomed in areas focusing on the IH-system and the PM-structure.

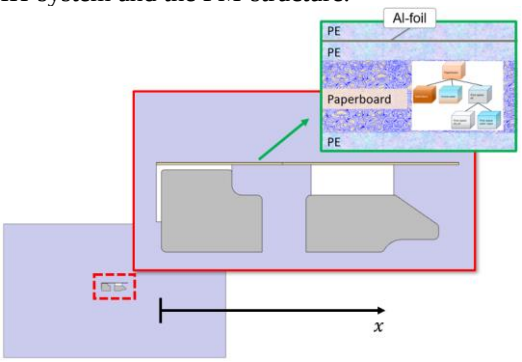

Figure 5. Computational domain; Lower Left) Entire domain needed for Magnetic field simulations, Center) Zoom in on the virtual representation of the sub-system test, and Upper Right) Zoom in on the PM.

Implementation

Al-foil: induction heating and heat transport
The IH-system of the sub-system rig is implemented via the Magnetic Fields interface of the AC/DC module. At $f \approx 500$ kHz and room temperature, the skin depth of aluminum is ≈ 100 µm and the Al-foil is electromagnetically thin, (Al-foil thickness, th_{Al}, is in the µm range), whereas the aluminum inductor is electromagnetically thick (coil cross sections is in the cm-range). Therefore, the aluminum conductor is modeled as a *Single-Conductor Domain Coil* with a prescribed rms current, the primary current, and a *Reversed Current Direction domain* assigned to the "return path" cross section of the aluminum inductor (see Figure 3). Due to its thin nature, the Al-foil is instead modeled as a *Single-Conductor Boundary Coil*. The eddy currents on the Al-foil are assumed to form a closed circuit, with the same current magnitude back and forth and a zero net current is prescribed to the Al-foil.

To mimic the closed loop feedback system of the IH generator, a *Global Equation* is utilized. This

equation enforces the primary current to vary dynamically such that the total load power is kept constant during the heating pulse. In order to apply the *Global Equation* feature, two additional *Frequency-Domain* steps need to be inserted prior to Step1. Firstly, a step to initialize the electromagnetic problem without the *Global Equation* activated, and then a second step with the *Global Equation* feature included.

Joule heating is incorporated by adding the electromagnetic surface loss power, $Q_{IH} \cdot th_{Al}$, as a boundary Flux/Source to the heat equation of the Al-foil. Finally, the heat equation of the Al-foil is expanded with a boundary *Weak Contribution*, implementing the equation for heat flux in *Thermally-Thin Layers* as reported [6].

Paperboard: heat and mass transport
The four equations, governing the response of the paperboard, are implemented as *General form PDE's* as described in Table 1, and with the standard COMSOL notations;
a: Dependent variables, Γ: Conservative flux
f: Source term, d_a: Damping Coefficient.

Table 1. Implementation of the governing equations of the Paperboard MT model as COMSOL Multiphysics - General Form PDE's.

nr	a	**Γ**	F	d_a
1	ω	**0**	$-\hat{m}_{s:g}$	$\rho_s n_s$
2	p_{g_a}	$\mathbf{J}_{g_a}$	$\frac{n_g \rho_{g_a}}{\theta}\dot{\theta}$-$\rho_{g_a}\dot{n}_g$	$\frac{n_g \rho_{g_a}}{p_{g_a}}$
3	p_{g_v}	$\mathbf{J}_{g_v}$	$\frac{n_g \rho_{g_v}}{\theta}\dot{\theta}$-$\rho_{g_v}\dot{n}_g + \hat{m}_{s:g}$	$\frac{n_g \rho_{g_v}}{p_{g_v}}$
4	θ	$\boldsymbol{q}_\theta^{MT}$	$-\hat{m}_{s:g}\Delta H_{s:g}$	ρc^p

PE-layers and Biadhesive tape thermal response
The thermal response of the polymers is implemented by adding *general form PDEs* to PDE 4, in Table 1. As for the PE layers, the polyethylene material from the COMSOL material library is adopted and for the biadhesive tape heat transport parameters corresponding to acrylic are assumed.

Initial values
Initial values are presented in Table 2.

Table 2. Initial values assumed for the primary variables.

ω^0	$p_{g_a}^0$	$p_{g_v}^0$	θ^0
0.074	$p_g^* - p_{g_v}^0$	$a_\omega^0 \cdot p_{g_v}^{sat}(\theta^0)$	θ^*

The initial water activity, $a_\omega^0 = a_\omega(\omega^0, \theta^0)$ [−], is modeled with the Oswin II isotherm in [5], the saturation vapor pressure, $p_{g_v}^{sat}(\theta^0)$ [Pa], is described with an Antoine relation and p_g^* [Pa] and θ^* [K] are the ambient pressure and temperature.

Boundary conditions
The mass fluxes, $J_{g_j}^n$, of the gas constituents, through the free edges of the board (vertical edges in Figure 3), are approximated by stagnant-film models with the incorporation of Stefan correction factors, as described in [7]. No heat flux is assumed on the contact between the biadhesive tape and the aluminum coil. All boundaries between polymers and ambient air assume a Newton cooling format with the heat convection coefficient, h_α, retrieved from classic boundary layer theory. The heat flux, q_θ^n, through the free edges of the board, incorporates the mass flux and is given by

$$q_\theta^n = h_\alpha(\theta - \theta^*) + J_{g_v}^n \cdot h_{g_v} + J_{g_a}^n \cdot h_{g_a}$$

where h_{g_j} [J/kg] is the specific enthalpy of g_v.

As for the magnetic field, a large computational domain is chosen, see Figure 5, and a magnetic insulation is assumed on the external boundaries.

Finally, during Step 1) a total load power of ~ 650 W is applied to the IH system

Results

The distribution of the norm of the magnetic field, $\boldsymbol{B}$, is shown in Figure 6 together with contour lines of the out-of-plane component of the magnetic vector potential, A_z.

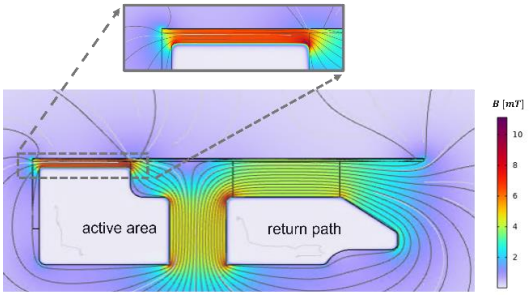

*Figure 6 Colorbar: norm of magnetic flux density **B** [mT]; contour lines: out-of-plane component of magnetic vector potential A_z [Wb/m²]. A magnified view is included to highlight the significant proximity effect.*

The contour lines of A_z produce closed circles around each coil cross-section, indicating that the currents in the active area and in the return path follow opposite directions. A significant proximity effect characterized by a high $\boldsymbol{B}$-norm is visible between the coil cross sections, and in between Al-

foil and the coil active area. The effect is caused by the opposite directions of the currents in coil and Al-foil.

The electromagnetic surface loss, $Q_{IH} \cdot th_{Al}$, computed by the *Magnetic Fields interface* (resistive loss contributions only) at the initial time step of the heating transient is shown in Figure 7.

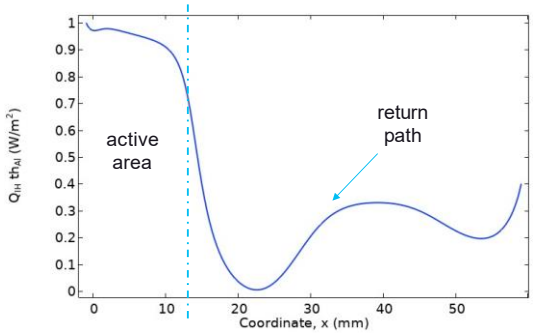

Figure 7. Induced surface loss density [W/m^2] (normalized to max.) on the Al-foil as a function of the x coordinate on the package material.

From Figure 7 it is observed how a higher surface loss density is applied in the region closer to the active area. The reason for this being both the closer distance between Al-foil and active area conductor as well as the smaller width of this conductor compared to the return path.

The predicted maximum temperature on the inside surface of the PM is shown in Figure 8 together with experimental data from [3].

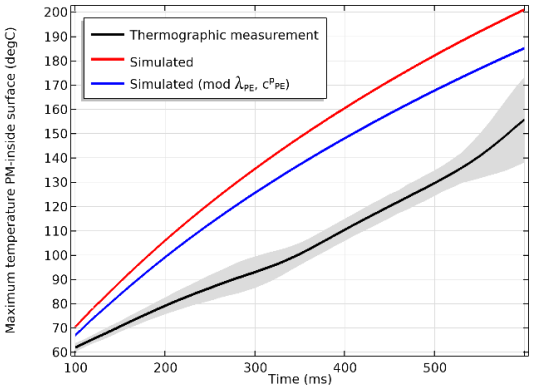

Figure 8 Evolution of the maximum temperature on inside surface. Black) Thermographic measurements, [3], (shading 3 std), Red) Simulation, Blue) Simulation with modified polymer heat transport properties.

A clear discrepancy between simulation and experimental measurements is observed. This discrepancy is attributed to simplifications and approximations made in both simulations and experimental measurements. The aim of this paper is not to scrutinize these and end up with a perfect match between model and measurements. However, one example is still given to exemplify the effect of the simplifications. The simulation assumes constant heat transport parameters for the polymer layers and the effect of this is illustrated through an additional simulation made with modified heat transport parameters. The modified heat transport parameters include a simplified temperature dependence of the thermal diffusivity of PE and from Figure 8 it is seen that this modification does not render a perfect correlation neither, but the discrepancy is clearly reduced.

Sensitivity study

To test the capability and robustness of the model a sensitivity analysis is performed. This analysis is made as an *All combinations - Parametric Sweep* with the input values posted in Table 3.

Table 3 Parametric Sweep of initial values.

Parameter	Value list	Unit
ω^0	0.04, 0.07, 0.1	1
ρ^c	500, 700, 900	kg · m^{-3}

The superscript $(\cdot)^c$, is used to express a material quantity when conditioned in RH = 50% and T = 23 °C. Note that the board density may be expressed in the volume fractions, n_α, and the component densities as $\rho^c = n_s^c \rho_s^c + n_l^c \rho_l^c + n_g^c (\rho_{g_a}^c + \rho_{g_v}^c)$. This implies that the different values of ρ^c will render different partitions of the three volume fractions. As shown in, e.g., [8] [9] [10], [11] and [2], several of the constitutive parameters are functions of the volume fractions, e.g., a high density will increase the thermal conductivity and decrease the gas permeability.

The maximum temperature on the inside surface is, for the heating phase, shown in Figure 9.

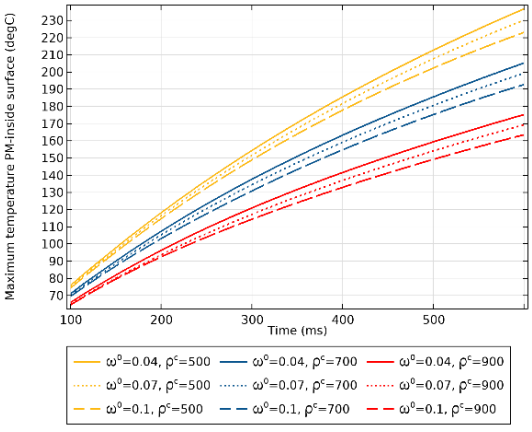

Figure 9. Evolution of the maximum temperature of the top surface of the paperboard.

From Figure 9 it is clear that using an IH system with a fixed "power supply" will render a lower inside temperature for a PM with a high density board, compared to a low density board, given that they have the same thickness. This is not surprising as a denser board is able to store more energy and has an increased thermal conductivity. It is also observed that it is more difficult to heat a moist PM. This is expected and attributed to increased effective thermal conductivity and volumetric heat capacity of the board as well as to energy required to dry the board.

One of the key benefits of using a multiphysics model is that it enables understanding of couplings which are otherwise difficult to comprehend. Two examples of such couplings are how the drying and the internal gas pressure, in the pore space of the board, are affected by ρ^c and ω^0. In Figure 10, the drying is illustrated with an absolute measure given by the minimum of $\omega^0 - \omega$ over the entire domain occupied by the board.

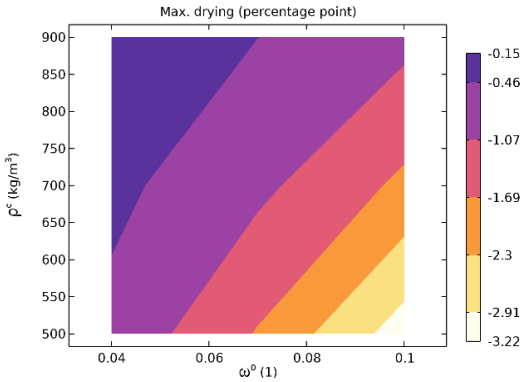

Figure 10 Illustration of how the maximum local drying is affected by the conditioned density ρ^c and the initial moisture ratio ω^0 of the board.

The drying is of a local nature and the maximum drying is found on the top left corner of the board domain, just below the Al-foil. It is observed that more moisture desorbs if the board has a higher initial moisture ratio and also if the board is less dense. Two reasons behind this observation are; 1) increasing ω^0 leads to an increased driving force for drying and thus increase the drying rate, 2) decreasing ρ^c will increase the volume of the pore gas which allows for the gas to accumulate more water and also ease the vapor transport within the board. The drying presented in Figure 10, is calculated at the end of the heating phase, t = 0.6 s. The dynamic nature of the drying is shown in Figure 11 for three of the parametric sweep simulations.

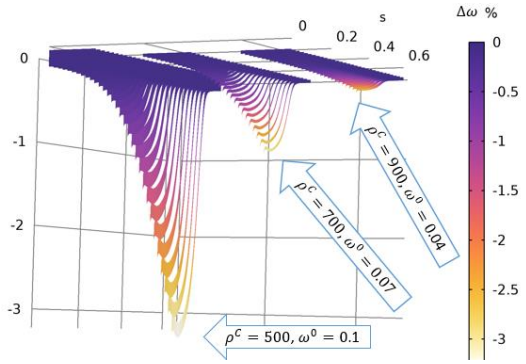

Figure 11. Evolution of the drying at the top surface of the board, over the coil active area. Data shown for three of the simulations from the parametric sweep.

The internal pressure build-up is illustrated, in Figure 12, with the maximum gauge pressure over the domain occupied by the board.

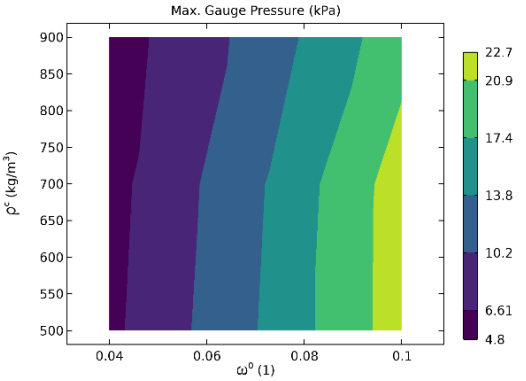

Figure 12. Illustration of how the maximum local gauge pressure is affected by the conditioned density ρ^c and the initial moisture ratio ω^0 of the board.

It is seen that the gauge pressure increases with ω^0 which is explained by the discussed increase in desorption. More surprisingly, the gauge pressure seems to decrease slightly with ρ^c. Increasing ρ^c will increase the resistance for the gas flux within the board and this will lead to a higher gauge pressure. However, remembering the results presented in Figure 9, i.e., an increase of ρ^c rendered a lower temperature in the board, it is concluded that the temperature has a more dominant influence on the gauge pressure, compared to the mass flux resistivity.

Numerical performance

The presented 2-D model contains ~ 2 M degrees of freedom and a single parametric run was solved in ~ 1 h using a state-of-the-art workstation with 8 cores or ~ 20 min when employing a cluster node with 24 cores. A good convergence was retrieved and the following actions aided in this; 1) The skin depth mesh in the inductor features 4 boundary

layers with thickness equal to half of the skin depth in aluminum, 2) A robust mapped mesh in the package material, an element size of, ~ 1/20 of the board thickness, and 3) Adopting a Fully-coupled approach to the Frequency-Transient study step, with a Jacobian update set to “Once per time step”.

Conclusions

COMSOL Multiphysics is used to analyze the response of PM during induction heating. A model is built by integrating the coupled heat and mass transport within PM with electromagnetic induction. The model is able to capture complex multiphysical couplings such as the gauge pressure build up and how this is affected by the density and initial moisture ratio. Due to simplifications and approximations made in both simulations and experiments, the model is, in its current state, unable to replicate physical temperature measurements. The next step in the model development is to improve the heat transport model for the polymer layers of the PM.

References

[1] R. Wool, B. L. Yuan and O. McGarel, "Welding of Polymer Interfaces," *Polymer Engineering and Science*, vol. 29, no. 19, pp. 1340 - 1367, 1989.

[2] H. Askfelt and M. Ristinmaa, "Experimental and numerical analysis of adhesion failure in moist packaging material during excessive heating," *International Journal of Heat and Mass Transfer*, vol. 108, pp. 2566 - 2580, 2017.

[3] M. Giangolini, G. Betti Beneventi and A. Babini, "Assessment of thermographic tools for the validation of physics-based models of an induction sealing process," *International Journal of Applied Electromagnetics and Mechanics*, vol. 75, no. 2, pp. 179-191, 2024.

[4] E. Kriezis, T. Tsiboukis, S. Panas and J. Tegopoulos, "Eddy currents: theory and applications," *Proceedings of the IEEE*, vol. 80, no. 10, pp. 1559-1589, 1992.

[5] J. Tryding, H. Askfelt, M. Alexandersson and M. Ristinmaa, "A full-range moisture sorption model for cellulosebased materials yielding consistent net isosteric heat of sorption," *Drying Technology*, 2022.

[6] "COMSOL Documentation - Heat Transfer Module Users Guide," 2023. [Online]. Available: https://doc.comsol.com/. [Accessed 2024].

[7] M. Alexandersson and M. Ristinmaa, "Coupled heat, mass and momentum transport in swelling cellulose based materials with application to retorting of paperboard packages," *Applied Mathematical Modelling*, vol. 92, pp. 848 - 883, 2021.

[8] L. Nilsson and S. Stenström, "Gas diffusion through sheets of fibrous porous media," *Chemical Engineering Science*, vol. 50, no. 3, pp. 361 - 371, 1995.

[9] L. Nilsson and S. Stenström, "A study of the permeability of pulp and paper," *International Journal Multiphase Flow*, vol. 23, no. 1, pp. 131 - 153, 1997.

[10] M. Karlsson and S. Stenström, "Static and Dynamic Modeling of Cardboard Drying Part 1: Theoretical Model," *Drying Technology*, vol. 23, pp. 143 - 163, 2005.

[11] I. Kartovaara, R. Rajala, M. Luukkala and K. Sipi, "Conduction of heat in paper," in *Papermaking Raw Materials, Trans. of the VIIIth Fund. Res. Symp. Oxford*, 1985.